멤브레인(Membrane Journal)
Vol. 30 No. 1 February, 2020, 66-77

Print ISSN: 1226-0088
Online ISSN: 2288-7253
DOI: https://doi.org/10.14579/MEMBRANE_JOURNAL.2020.30.1.66

비틀린 중공사막이 모듈에 미치는 영향: 전산 유체역학 시뮬레이션을 통한 정삼투 모듈의 압력과 농도 분포

김 수 헌 · 이 철 민 · 김 인 수†

광주과학기술원 지구환경공학부

(2019년 12월 23일 접수, 2020년 2월 10일 수정, 2020년 2월 24일 채택)

Effect of Twisted Hollow Fiber Membranes in a Module: Computational Fluid Dynamics Simulations on the Pressure and Concentration Profile of the Module in the forward Osmosis

Suhun Kim, Chulmin Lee, and In S. Kim†

School of Earth Sciences and Environmental Engineering, Gwangju Institute of Science and Technology (GIST), 123 Cheomdangwagi-ro, Buk-gu, Gwangju 61005, Korea

(Received December 23, 2019, Revised February 10, 2020, Accepted February 24, 2020)

요 약: 본 연구에서는 정삼투 중공사막 모듈에서 중공사막의 가닥을 비틀어 배치하였을 때의 효과를 알아보기 위해 CFD 전산 유체 역학 프로그램을 통해 5개의 다른 각도로 비틀린 중공사막 모듈을 설계하고 시뮬레이션하여 비틀리지 않은 모듈과 비교하였다. 실험 결과, 중공사막이 비틀렸을 때, 모듈 내부의 유도 용액의 농도가 비틀리지 않을 때에 비해 고르게 분포하였다. 모듈 입구의 압력은 중공사막의 비틀림과 관계없이 일정한 값을 보였지만 출구의 압력은 중공사막이 비틀린 정도가 커질수록 증가하는 추세를 보였다. 출구의 압력이 높아짐에 따라 막 내부의 유체 속도가 감소하고 모듈 체류 시간이 증가하여 막 사이의 물질 교환이 원활하게 이루어질 것으로 예측된다. 이는 결과적으로 막이 비틀려 있을 때의 모듈 플럭스가 투과 수량이 차지하는 비율이 그렇지 않을 때에 비해 2배 증가하였다.

Abstract: The current study focused on the effect of twisting hollow fibers (HFs) in a module during forward osmosis operation mode. Computational fluid dynamics simulation was employed for a straight HF module and twisted modules with five different angles to predict the mass transfer and observe the draw solution profile in terms of concentration and pressure. The simulation results showed that when the membranes were twisted, the concentration was distributed more evenly and the pressure at the module outlet increased gradually as the twisting angle increased. As pressure at the outlet increased, the fluid velocity inside the membrane decreased and the residence time of fluid increased, thereby facilitating mass exchange across the membrane. This is evidenced by a doubling of the ratio of water flux through the membrane in module flux when the HFs were twisted.

***Keywords**: twisted hollow fiber, hollow fiber module, forward osmosis, computational fluid dynamics*

1. Introduction

Forward osmosis (FO) is a water treatment process based on membrane filtration that has a wide range of applications for wastewater treatment, desalination, and food processing in academic research and industry[1-9]. In the FO process, water is transported by the chemical potential that results from the concentration difference between the diluted feed solution and the concentrated draw solution through a semi-permeable membrane[10-14]. Unlike desalination processes that rely upon pressure or heat, such as reverse osmosis (RO) or

†Corresponding author(e-mail: iskim@gist.ac.kr, http://orcid.org/0000-0002-6016-5267)

membrane distillation (MD), water transfer in FO is spontaneous, which can minimize external energy input. In addition, membrane fouling may be remarkably reduced because almost no hydraulic pressure is applied, unlike other processes. Thermodynamically, FO desalination cannot directly save energy in absolute terms, but it is expected to greatly improve the performance of RO or heat-treatment desalination processes and to reduce operating costs when properly applied to hybrid processes in combination with other processes[15].

Hollow fibers (HFs) have been used in FO membranes prior to the commercialization phase[16,17]. HF membranes have been applied in various fields, such as drinking water and waste water treatment. HF is competitive with other membrane configurations because (1) the mechanical properties of HFs in the module or contactor mean that they do not require spacers, and (2) HFs have a higher packing density and a high effective membrane surface area. As a result of those advantages, HF modules have entered the spotlight, but they have the disadvantage of undergoing severe damage even at low concentrations of contaminants[18]. In order to understand the advantages and disadvantages of HF FO modules and to improve their performance, it is necessary to understand the characteristics of the fluid inside the module.

However, it is practically impossible to understand fluid flow inside the module through experiments. Therefore, we employed computational fluid dynamics (CFD) to simulate both flow characteristics and mass transfer phenomena by solving and analyzing problems related to fluid flow. CFD can be a useful tool for predicting the effects that features have on hydrodynamics at a fundamental level of module design to improve upon these negative aspects of FO membranes and to provide guidance on effective module design[19-23]. Through its advantages, CFD provides a way not only to incorporate the effects of individual characteristics such as solute rejection, membrane slip velocity, and the membrane water flux into one model, but also to apply them to the hydrodynamic conditions of flow channels around the membrane[24-26]. It can be used to explain the realistic details of the flow field on a fine scale.

A few of HF module studies previously have attempted to twist HF membranes inside the module as to improve the performance. However, those studies were simulated to aim at reverse osmosis process[27] or to analyze effects due to change of operating conditions[28] or to examine incompressible flow through twisted elliptical hollow fiber membrane[29]. In this study, we focused on changes in the fluid dynamics and solution profile, such as the pressure and concentration of the module, due to the degree of twisting between hollow fibers assuming an FO process. For this purpose, a CFD model was designed to investigate the relationship between module design and fluid flow changes according to the internal structure of the module, operating under the assumption that the shell side corresponds to the draw solution and the lumen side to the feed solution.

2. Experimental Methods

2.1. Simulation conditions

The twisting angle of HF was defined as the included angle between the straight line drawn from the head of HF to the center of the module and the straight line drawn from the center of the module to the tail of HF. In the simulation, the bundles of hollow fiber membranes were twisted at 0, 15, 30, 45, 60, and 90°, and the concentration, pressure, and flux distribution were compared across these conditions. A 35 g/L NaCl solution was used as the draw solution of the module to reflect assumed seawater conditions. This simulation represented the FO process of hollow fibers as consisting of a lumen (on the interior side of the HFs) of pure water as feed water and a shell (on the exterior side of the HFs) containing a draw solution made up of 35 g/L NaCl. We also determined that the water flux would be low due to the small module size and concerning internal concentration polarization, and conducted the simulation under the assumption that the flux of the entire membrane surface

Table 1. Parameters Input for The Simulation

Parameter		Value
Geometrical parameters	Diameter of hollow fiber membrane: d	0.004 m
	Diameter of module: D	0.07 m
	Length of module: L	0.3 m
	Twisting angle	0°, 15°, 30°, 45°, 60°, 90°
Physical properties	Kinematic viscosity of water: v	0.8926 mm^2/s
	Dynamic viscosity: μ	0.001 Poise
	Temperature: T	298.15 K
	Density of water: ρ	0.998 g/cm^3
Operating conditions	Number of fibers	137
	Concentration of NaCl draw solution: C_D	35 g/L NaCl

area was constant because the unbalanced distribution of flux of HF membrane is negligible due to the module is small in size. Based on this assumption, it was expected that the concentration change inside the module is insignificant because the factors that affect the concentration of solution inside the module such as the composition conditions and the membrane permeate are not large. Therefore, the concentration change of the solution was excluded.

Our goal was to observe the flow characteristics of the solution outside of the HFs in the module. The numerical method used in this study was the finite element method (FEM), in which partial differential equations such as Navier-Stokes and the mass conservation equation were represented and evaluated. The calculations were done with the minimum root mean square set at 10^{-4}. The mesh configuration of the module was created by ANSYS 19.1. Meshing based on the general grid interface connections and the governing equations were computed numerically through the CFD Solver in ANSYS 19.1.

Table 1 shows the modeling parameters used in this study, following[30].

The fluid flow was set as pure laminar flow and all boundaries around the rest of the domain were set as non-slip walls to assume a dead-end module operation. The nominal velocity of NaCl solution at the module inlet was set at 0.0167 mm/s and the static pressure at the module outlet was set at 0 bars. In the calculations, 0.8926 mm^2/s was set as the kinematic viscosity (ν) of pure water, because the kinematic viscosity of 35 g/L NaCl solution is not substantially different from that of pure water[31]. The fluid temperature was set at 298.15K, isothermally.

2.2. Governing equations

We assumed a Newtonian fluid, and the flow was assumed to be laminar. As an incompressible fluid in a steady state, the fluid model was governed by the Navier-Stokes and conservation of mass equations. To analyze fluid movement, these equations are expressed with constant physical properties, as follows:

$$(\vec{v} \cdot \nabla)\vec{v} = -\frac{1}{\rho}\nabla P + v\nabla^2\vec{v} \quad (1)$$

$$\nabla \cdot \vec{v} = 0 \quad (2)$$

Where $\vec{v}$ is the velocity vector with components in the x, y, and z directions, v is kinematic viscosity, P is static pressure, and ρ is density. In this study, the pure water density at 25°C was set as 0.998 g/m^3[32].

To consider the migration phenomenon of seawater, a solution-diffusion membrane transport model was assumed. The salt concentration field was expressed by the mass transport equation, and the concentration gradient though the membrane element was analyzed as:

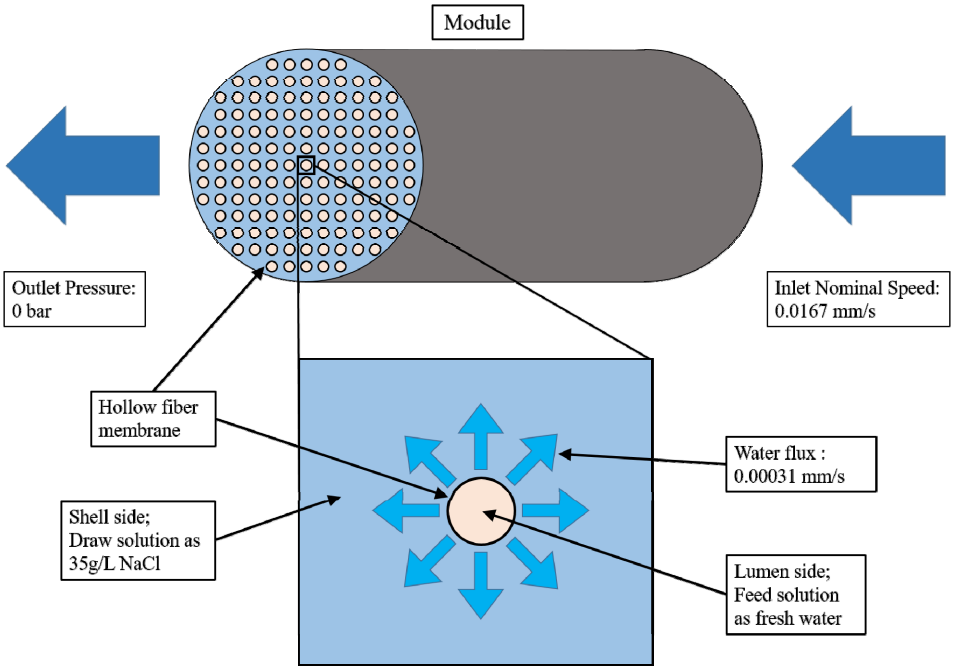

Fig. 1. Schematic diagram of operating and boundary conditions. The boundary condition of the module as inlet nominal speed of NaCl solution was 0.0167 mm/s of and outlet pressure was 0 bar. The boundary condition of the hollow fiber membranes as the water flux though the hollow fiber membrane was 0.00031 mm/s.

$$(\vec{v} \cdot \nabla)c = D\nabla^2 c \tag{3}$$

$$D\nabla c \cdot \vec{n} = \vec{v} \cdot \vec{n}(c_w - c_p) \tag{4}$$

Where C is the salt concentration, D is the diffusion coefficient, $\vec{n}$ is the unit vector normal to the surface, $\vec{v} \cdot \vec{n}$ stands for the local water flux through the HF membrane surface, c_w is the local salt concentration along the membrane surface, and c_p is the salt concentration on the production side (equaling zero).

2.3. Structure of the module

The overall structure of the module was designed with reference to the commercialized HF FO module HFFO2 (Aquaporin, Denmark)[33,34]. The module used in the simulation was a cylindrical shape with evenly-packed HFs. Its length was 0.3 m and its diameter was 0.07 m. The length of the HFs constituting the module was 0.3 m and their diameter was 0.004 m. The spacing between the HFs was 0.005 m from the center of the membrane, and the module contained 137 fibers.

The draw fluid entered the domain in the -x direction, normal to the vertical inlet face. The inlet and outlet faces were parallel, and inlet face was defined as a pressure inlet. Therefore, all fluid entering the domain flowed in through the inlet face and out through the outlet face. The operating and boundary conditions are shown in Fig. 1. Also, Fig. 2. illustrates the designed module and explanation of the definition of twisting angle of HF, which had angles of twisting of 0° as a control, and 90°. The bottom right side of the picture shows the inlet face and the top left side shows the outlet face. In the front view of the straight module, there are empty spaces were shown due to the head and tail of HF are straight. It could be seen through the straight green line clearly in the diagonal view of the module. In contrast, in the view of 90° twisted module, the position of HF tail (green rim) was twisted 90° clockwise than the position of HF head (green circle). This is, as defined by the twisting angle, the angle between the line from HF inlet to the center of

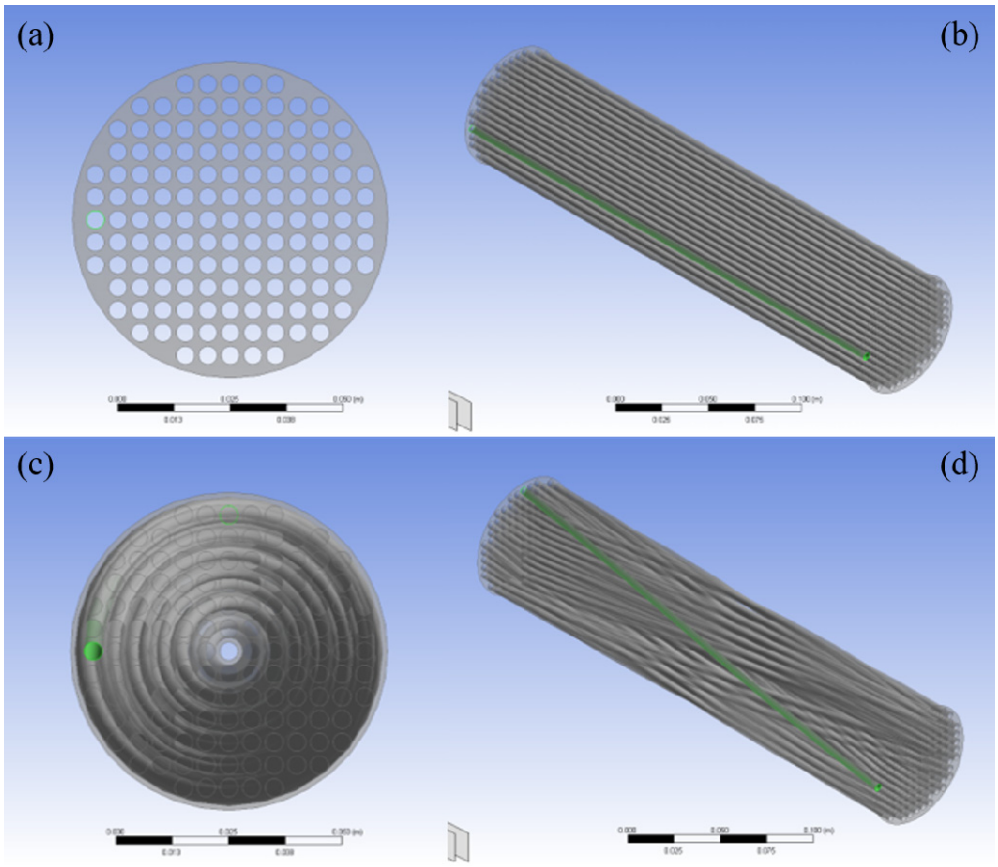

Fig. 2. Illustration of the module design. (a) the front view of the straight module, (b) the diagonal view of straight module, (c) the front view of the 90° twisted module, and the (d) the diagonal view of 90° twisted module.

module (the line between the green circle and the transparent hole) and the line from the center of module to the HF outlet (the line between the transparent hole and the green rim) were 90°. This could be seen through the twisted green line clearly in the diagonal view of the 90° twisted module.

The total membrane area of the module was 0.5165, 0.5163, 0.5165, 0.5167, 0.5171, and 0.5182 m^2, respectively, for the six angles of twisting. The membrane area did not meaningfully change with the angle of twisting, with values ranging only slightly from 0.516 to 0.518. Compared to the 0° twisted state, the increments were only 0.03, 0, 0.05, 0.12, and 0.33%, respectively, as the angle increased.

3. Results and Discussion

3.1. Concentration profile of the NaCl draw solution

The concentration profiles of the straight HF module and the five twisted HF modules are illustrated in Fig. 3. The water influx from the membrane into the module was steady, so the concentration of draw solution around the membrane was lower. When the HFs were not twisted, the concentration of NaCl solution gradually increased from the module inlet to the end of the module. The peak concentration at the module outlet was 79.64 g/L, and the highest concentration inside the module was 82.97 g/L. In addition, the standard deviation of the concentration distribution inside the module was 13.43 g/L.

However, when the HFs were twisted, the concen-

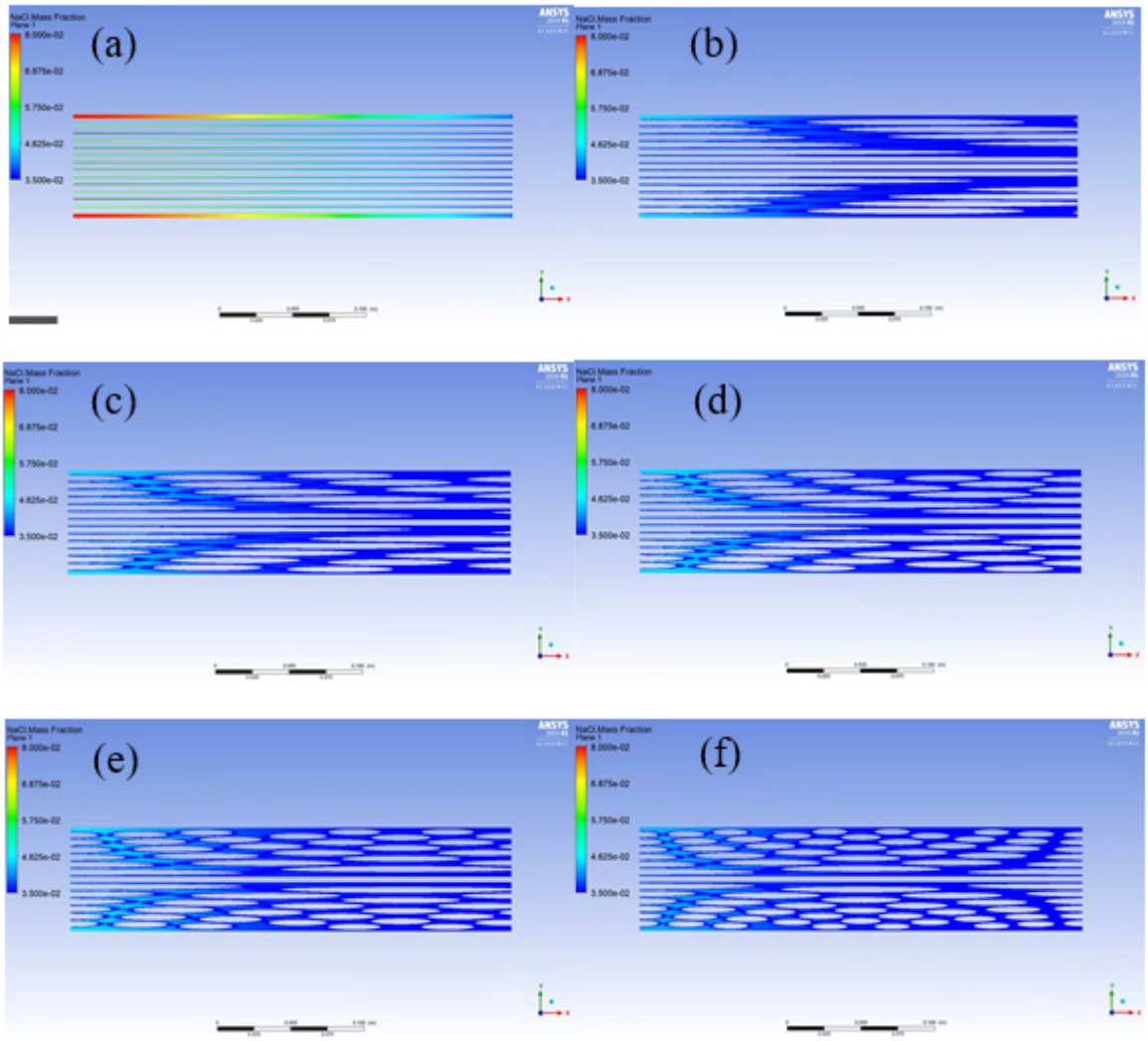

Fig. 3. Illustrations of the concentration profile. (a) 0°, (b) 15°, (c) 30°, (d) 45°, (e) 60°, and (f) 90° twisted modules, respectively.

tration of the NaCl solution was distributed more evenly than when they were not twisted, at around 45 g/L. The peak concentrations at the module outlet according to the angle of twisting, from 15° to 90°, were 44.96, 45.09, 45.32, 45.25, and 42.49 g/L, respectively. Furthermore, the highest concentrations inside the module were 45.94, 46.08, 46.32, 46.24, and 43.36 g/L, respectively. The standard deviations were 3.26, 3.28, 3.37, 3.33, and 2.48 g/L, respectively, for each angle of twisting.

Compared to when the HFs were not twisted, the peak concentration inside the module decreased when the HFs were twisted, and the standard deviation of the concentrations also decreased. As the HFs were twisted, the alternating internal structure of the module created a vortex of fluid that prevented the stagnation of NaCl particles that would otherwise occur when the HFs were not twisted. The vortex flow structure created by twisting HF adds cross flow to the existing fluid flow along the axis and prevents jet flow that quickly exits the module without interruption. This could be attributed to the increase in momentum mixing due to the increased shear stress on the membrane surface as twisting HF. It could be understood that the

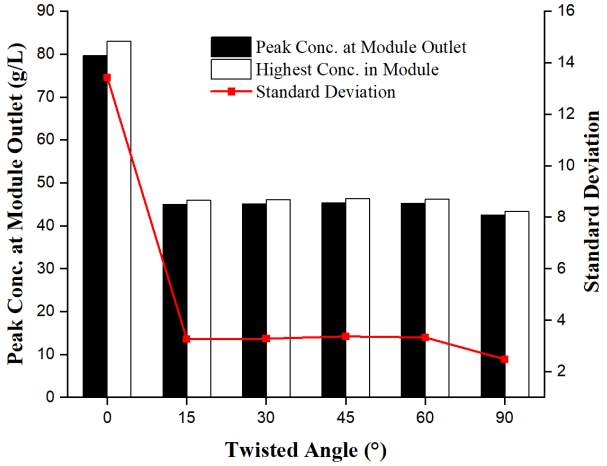

Fig. 4. Changes in the concentration of the NaCl solution in response to changes in the angle of HF twisting inside the module. The black bars indicate the peak concentration at the module outlet, and the white bars indicate the highest concentration in the module. The red line is the standard deviation of the concentration.

increased shear stress on the membrane helps to distribute the solution from the farthest part of the membrane closer to the membrane, helping to evenly distribute the solution concentration inside the module. As a result, the vortex makes the fluid movement inside the module more complex, pushing out stagnant NaCl particles, evenly distributing the draw solution concentration, and preventing high concentrations. Therefore, the peak concentration and the standard deviation of the concentration both decreased.

Fig. 4. is a graph drawn according to the peak concentration at the module ends and the highest concentration of NaCl draw solution in the module with standard deviation for the six angles of twisting. When the HFs were twisted, the draw solution was distributed more evenly than when the HFs were not. Additionally, the peak concentration was significantly lower when the HFs were twisted, regardless of the angle. There is no significant difference in these results from 15° to 90° because the internal structure does not change much with angle of twisting. This suggests that twisting membranes can achieve a uniform distribution of the draw solution concentration inside the module. Even small angles of twisting resulted in a markedly more uniform concentration.

3.2. Pressure profile of the module

The FO process does not involve direct pressure on the membrane; however, naturally-occurring pressure could be applied on the membrane surface through the action of the pump that circulates the solution. If this pressure is sufficiently small compared to the osmotic pressure, it has a negligible impact on the operation of the module. However, when this pressure is not sufficiently small, it prevents efficient operation of the module. The pressure profiles of the straight HF module and the five twisted HF modules are illustrated in Fig. 5. It shows the pressure gradient of module and pressure at inlet and outlet.

Fig. 6. is a graph presenting the inlet and outlet pressure of the modules with six angles of twisting. Regarding the inlet pressure, when the HFs were not twisted, the pressure applied was 6.282×10^{-3} Pa, while when the HFs were twisted, the applied pressure according to the angle of twisting from 15° to 90° was 6.693×10^{-3}, 6.679×10^{-3}, 6.698×10^{-3}, 6.733×10^{-3}, and 6.841×10^{-3} Pa, respectively. The inlet pressure increase due to membrane twisting was negligibly small, and there was no correlation between the angle of membrane twisting membrane and the pressure. It was anticipated that the pressure applied at the module inlet would increase due to the change in the movement of the fluid caused by membrane twisting, but the simulation results showed no significant increase.

However, the outlet pressure was increased by membrane twisting. The pressure applied at the straight module was 2.095×10^{-9} Pa, and the outlet pressure in the twisted module was 4.515×10^{-7}, 4.842×10^{-7}, 5.190×10^{-7}, 5.560×10^{-7}, and 6.220×10^{-7} Pa, respectively. The outlet pressure increased more as a result of membrane twisting than the inlet pressure did, and a positive relationship was found between the angle of membrane twisting and the outlet pressure.

As a result, the pressure at the module inlet was constant, but the pressure at the module outlet increased, which could lead to stagnation of the fluid in

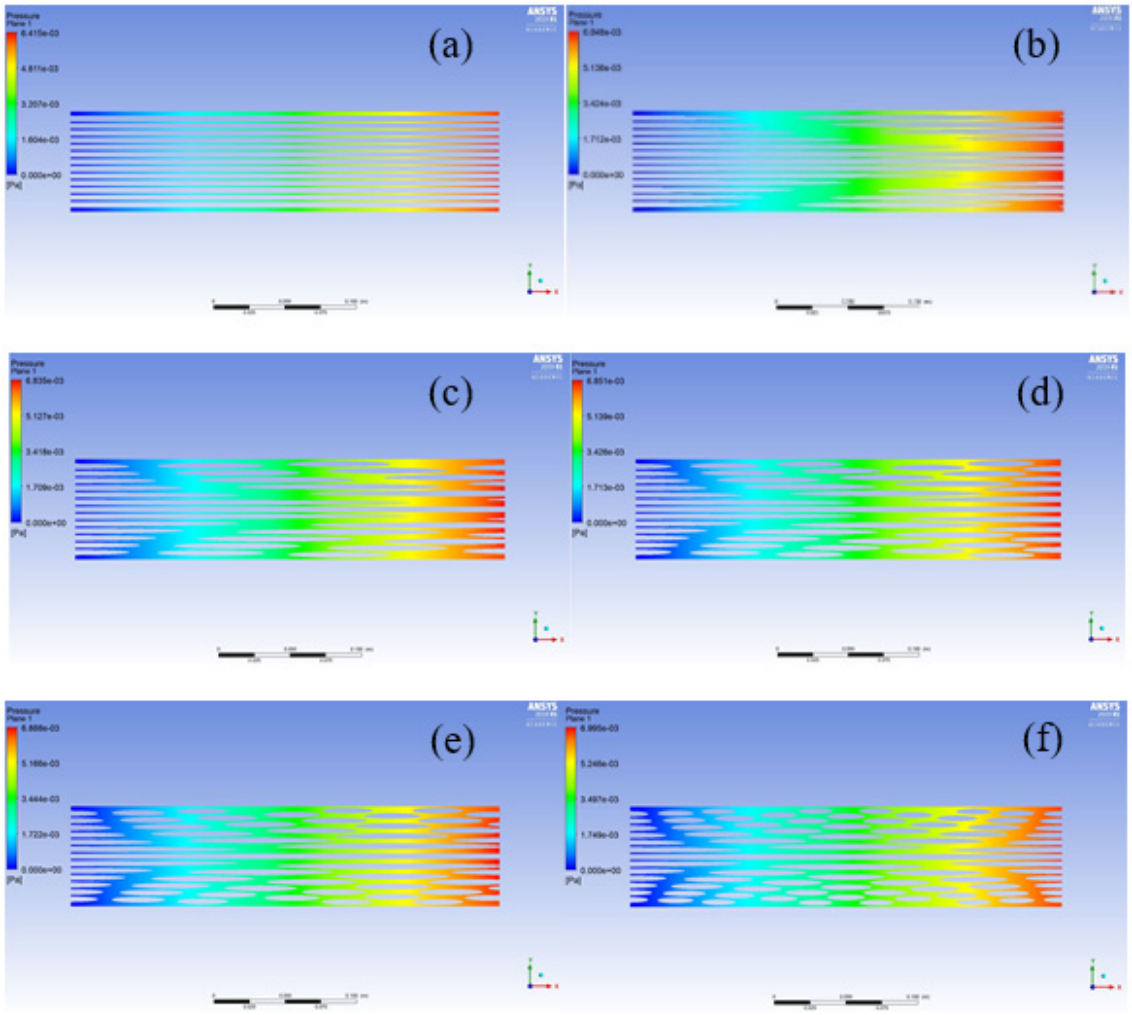

Fig. 5. Illustrations of the pressure profile. (a) 0°, (b) 15°, (c) 30°, (d) 45°, (e) 60°, and (f) 90° twisted modules, respectively.

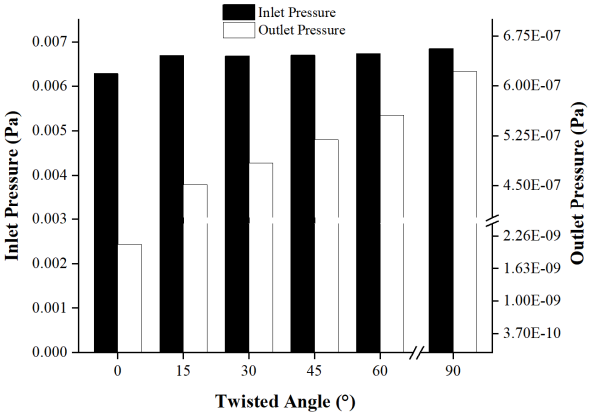

Fig. 6. Changes in the pressure applied at the module inlet and outlet due to changes in the angle of HF twisting inside the module. The black bars indicate pressure at the module inlet and the white lines indicate outlet pressure.

side the module. Therefore, when the flow of fluid inside the module is delayed, mass exchange across the membrane can occur smoothly. In addition, the concentration distribution inside the module became constant when the membrane was twisted, enabling it to be operated effectively without losing osmotic pressure.

3.3. Flux of the module

The mass flow of the module was analyzed to see how twisting the membrane affected the module flux. In order to compare the module performance under each condition, the ratio of membrane permeate to module outflow was calculated. Since the boundary conditions of the module inlet did not change, changes at the out-

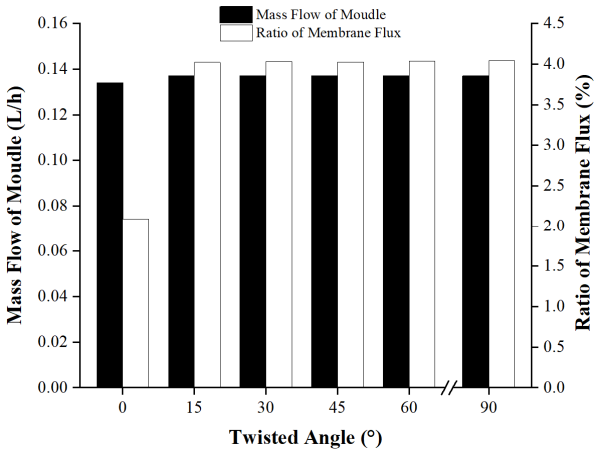

Fig. 7. Change of mass flow at the module outlet and the ratio of membrane flux due to changes in the angle of HF twisting inside the module. The black bars indicate the module mass flow, and the white bars indicate the ratio of membrane flux at the module outlet.

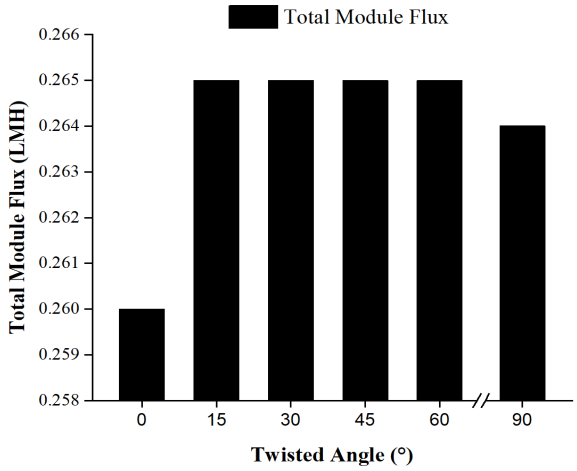

Fig. 8. Change in module flux due to changes in the angle of HF twisting inside the module.

let were observed. To calculate the ratio, this equation was expressed, as follows:

$$\frac{Membrane\ permeate\ into\ the\ module\ inside}{Mass\ flow\ of\ the\ module\ outlet} = \frac{(Mass\ flow\ of\ the\ module\ outlet)-(Mass\ flow\ of\ the\ module\ inlet)}{(Mass\ flow\ of\ the\ module\ outlet)} \quad (5)$$

The mass flow of the module inlet was 0.1314 L/h. Fig. 7. shows the mass flow at the module outlet and the ratio of membrane flux according to the simulation results. When the HFs were not twisted, the mass flow at the module outlet was 0.1342 L/h, while when the HFs were twisted, a constant value of 0.1369 L/h was found from 15° to 90°. The ratio of water flux that pass through the membrane in the straight module flux was 2.091%, and the ratios for the twisted modules were 4.022, 4.029, 4.026, 4.034, and 4.042%, respectively. Therefore, the mass flow of the module did not increase significantly, but compared to when the HFs were not twisted, the ratio of water flux pass through HF membranes in the mass flow of module was doubled when the HFs were twisted.

Fig. 8. presents a graphical visualization of the relationship between the total module flux and the angle of twisting. Module flux is the number of module out-flow divided by the total area of the HFs within the module with LMH (L/m^2/hour). This represents the volume of water that travels through the unit area (1 m^2) over a unit time (1 hour), making it easier to compare the performance of modules under different simulation conditions.

When the HFs were not twisted, the flux was 0.260 LMH, while when the HFs were twisted at angles between 15° and 60°, a constant value of 0.265 LMH was seen, and the 90° twisted module showed a flux of 0.264 LMH. Thus, the flux of the module was increased simply by twisting the HFs, without changing the membrane area. The total module flux shown in the simulation results has a huge difference between the straight module as 0° and the twisted module as 15°, and no significant change after the HF twisted. This is because the fluid resistance inside the twisted module is bigger compared with the straight module, and no difference in fluid resistance given by the twisting angle after HF twisted.

In response to HF twisting, the ratio of membrane permeate to module outflow increased by about two times, and the flux of the module also increased. This change occurred because the pressure at the outlet of the module increased and the velocity of the fluid inside the module decreased. Thus, when HF twisted, the

fluid velocity inside the module decreases and the ratio of the membrane permeate to mass outflow of the module increases, resulting in an increase in the total flux of the module.

4. Conclusions

This study presents a comprehensive CFD model that included changes in fluid characteristics (pressure and concentration) inside the module when HFs were twisted in the FO process. A module with 137 HF membranes twisted at six different angles, from 0° to 90°, was simulated and the simulated performance of each module was compared in terms of the concentration distribution of the NaCl draw solution and the pressure gradient of the module. The CFD simulation results indicated that when the HFs were twisted, the concentration was evenly distributed and the velocity of the fluid decreased. When the permeate of the membrane is constant and the inflow of the module is the same, twisting the HF membrane results in more mixing of the solution in the module and maintains the osmotic pressure to induce more permeate through the membrane. Compared to straight module, the effluent from the module was further diluted (with better dilution efficiency) and improved module flux. As a result, the performance of the FO module is improved. These CFD results can be used as one of indicators, suggesting directions and possibilities for improving HF FO module performance prior to demonstration experiments.

Acknowledgements

This work was supported by Korea Environment Industry & Technology Institute (KEITI) through Industrial Facilities & Infrastructure Research Program, funded by Korea Ministry of Environment (MOE) (1485016290) and (1485016165).

Reference

1. S. Zhao, L. Zou, C. Y. Tang, and D. Mulcahy, "Recent developments in forward osmosis: Opportunities and challenges", *J. Membr. Sci.*, **396**, 1 (2012).
2. D. Ma, S. B. Peh, G. Han, and S. B. Chen, "Thin-film nanocomposite (TFN) membranes incorporated with super-hydrophilic metal-organic framework (MOF) UiO-66: Toward enhancement of water flux and salt rejection", *ACS Appl. Mater. Interfaces.*, **9**, 7523 (2017).
3. S. Kook, C. D. Swetha, J. Lee, C. Lee, T. Fane, and I. S. Kim, "Forward osmosis membranes under null-pressure condition: Do hydraulic and osmotic pressures have identical nature?", *Environ. Sci. Technol.*, **52**, 3556 (2018).
4. A. J. Ansari, F. I. Hai, W. E. Price, J. E. Drewes, and L. D. Nghiem, "Forward osmosis as a platform for resource recovery from municipal wastewater - A critical assessment of the literature", *J. Memb. Sci.*, **529**, 195 (2017).
5. M. Zhan, G. Gwak, D. Inhyuk, K. Park, and S. Hong, "Quantitative analysis of the irreversible membrane fouling of forward osmosis during wastewater reclamation: Correlation with the modified fouling index", *J. Memb. Sci.*, **597**, 117757 (2020).
6. S. S. Manickam and J. R. McCutcheon, "Understanding mass transfer through asymmetric membranes during forward osmosis: A historical perspective and critical review on measuring structural parameter with semi-empirical models and characterization approaches", *Desalination*, **421**, 110 (2017).
7. E. Yang, C. M. Kim, J. Song, H. Ki, M. H. Ham, and I. S. Kim, "Enhanced desalination performance of forward osmosis membranes based on reduced graphene oxide laminates coated with hydrophilic polydopamine", *Carbon*, **117**, 293 (2017).
8. W. Xu, Q. Chen, and Q. Ge, "Recent advances in forward osmosis (FO) membrane: Chemical modifications on membranes for FO processes", *Desalination*, **419**, 101 (2017).
9. D. M. Warsinger, S. Chakraborty, E. W. Tow, M. H. Plumlee, C. Bellona, S. Loutatidou, L. Karimi, A. M. Mikelonis, A. Achilli, A. Ghassemi, L. P.

Padhye, S. A. Snyder, S. Curcio, C. D. Vecitis, H. A. Arafat, and J. H. Lienhard, "A review of polymeric membranes and processes for potable water reuse", *Prog. Polym. Sci.*, **81**, 209 (2018).
10. D. Xiao, W. Li, S. Chou, R. Wang, and C. Y. Tang, "A modeling investigation on optimizing the design of forward osmosis hollow fiber modules", *J. Memb. Sci.*, **392-393**, 76 (2012).
11. D. L. Shaffer, J. R. Werber, H. Jaramillo, S. Lin, and M. Elimelech, "Forward osmosis: Where are we now?", *Desalination*, **356**, 271 (2015).
12. C. M. Werner, B. E. Logan, P. E. Saikaly, and G. L. Amy, "Wastewater treatment, energy recovery and desalination using a forward osmosis membrane in an air-cathode microbial osmotic fuel cell", *J. Membr. Sci.*, **428**, 116 (2013).
13. R. V. Linares, Z. Li, S. Sarp, S. S. Bucs, G. Amy, and J. S. Vrouwenvelder, "Forward osmosis niches in seawater desalination and wastewater reuse", *Water Res.*, **66**, 122 (2014).
14. J. Jang, I. Park, S. S. Chee, J. H. Song, Y. Kang, C. Lee, W. Lee, M. H. Ham, and I. S. Kim, "Graphene oxide nanocomposite membrane cooperatively cross-linked by monomer and polymer overcoming the trade-off between flux and rejection in forward osmosis", *J. Memb. Sci.*, DOI:10.1016/j.memsci.2019.117684 (In press).
15. S. Lin, "Mass transfer in forward osmosis with hollow fiber membranes", *J. Memb. Sci.*, **514**, 176 (2016).
16. https://www.forwardosmosistech.com/the-4-different-designs-of-forward-osmosis-fo-membrane-modules/, March 30 (2014).
17. https://aquaporin.com/fo/, October 17 (2019).
18. https://www.forwardosmosistech.com/hollow-fiber-forward-osmosis-membrane-modules/, March 28 (2014).
19. M. Brannock, Y. Wang, and G. Leslie, "Mixing characterisation of full-scale membrane bioreactors: CFD modelling with experimental validation", *Water Res.*, **44**, 3181 (2010).
20. P. Sousa, A. Soares, E. Monteiro, and A. Rouboa, "A CFD study of the hydrodynamics in a desalination membrane filled with spacers", *Desalination*, **349**, 22 (2014).
21. A. Cahyadi, S. Yang, and J. W. Chew, "CFD study on the hydrodynamics of fluidized granular activated carbon in AnFMBR applications", *Sep. Purif. Technol.*, **178**, 75 (2017).
22. C. Lee, S. Kook, C. Choi, T. T. Nguyen, and I. S. Kim, "Effects of membrane envelope geometry on hydrodynamics inside draw channel of forward osmosis spiral wound membrane element", *Desalin. Water Treat.*, **112**, 282 (2018).
23. C. Choi, C. Lee, N.-S. Park, and I. S. Kim, "Numerical study of fluid behavior on protruding shapes within the inlet part of pressurized membrane module using computational fluid dynamics", *Environ. Eng. Res.*, DOI:10.4491/eer.2018.423 (In Press).
24. L. Zhuang, H. Guo, P. Wang, and G. Dai, "Study on the flux distribution in a dead-end outside-in hollow fiber membrane module", *J. Membr. Sci.*, **495**, 372 (2015).
25. F. Parvaza, S. H. Hosseinib, K. Elsayedc, and G. Ahmadid, "Numerical investigation of effects of inner cone on flow field, performance and erosion rate of cyclone separators", *Sep. Purif. Technol.*, **201**, 223 (2018).
26. F. Zhou, G. Sun, Y. Zhang, H. Ci, and Q. Wei, "Experimental and CFD study on the effects of surface roughness on cyclone performance", *Sep. Purif. Technol.*, **193**, 175 (2018).
27. M. Usta, M. Morabito, A. Anqi, M. Alrehili, A. Hakim, and A. Oztekin, "Twisted hollow fiber membrane modules for reverse osmosis-driven desalination", *Desalination*, **441**, 21 (2018).
28. M. Shibuya, M. Yasukawa, S. Goda, H. Sakurai, T. Takahashi, M. Higa, and H. Matsuyama, "Experimental and theoretical study of a forward osmosis hollow fiber membrane module with a cross-wound configuration", *J. Memb. Sci.*, **504**, 10 (2016).
29. S. P. Motevalian, A. Borhan, H. Zhou, and A. Zydney, "Twisted hollow fiber membranes for enhanced mass transfer", *J. Memb. Sci.*, **514**, 586

(2016).
30. W. M. Haynes, “CRC Handbook of Chemistry and Physics”, 93st ed., pp. 6-8, 6-231, CRC Press, Boca Raton, FL (2012).
31. G. Pereira, R. Moreira, M. J. Vázquez, and F. Chenlo, “Kinematic viscosity prediction for aqueous solutions with various solutes”, *Chem. Eng. J.*, **81**, 35 (2001).
32. L. Zhuang, H. Guo, G. Dai, and Z.-L. Xu, “Effect of the inlet manifold on the performance of a hollow fiber membrane module-A CFD study”, *J. Memb. Sci.*, **526**, 73 (2017).
33. https://aquaporin.com/wp-content/uploads/2019/08/Aquaporin-HFFO2-Datasheet.pdf, August 1 (2019).
34. https://aquaporin.com/wp-content/uploads/2019/11/Aquaporin-HFFO2-Standard-Test-Setup.pdf, November 1 (2019).